Cell Reports
Physical Science

Article

Thermal-mechanical triphasic assembly enables ultra-strong soy protein adhesives via biomass welding

Graphical abstract

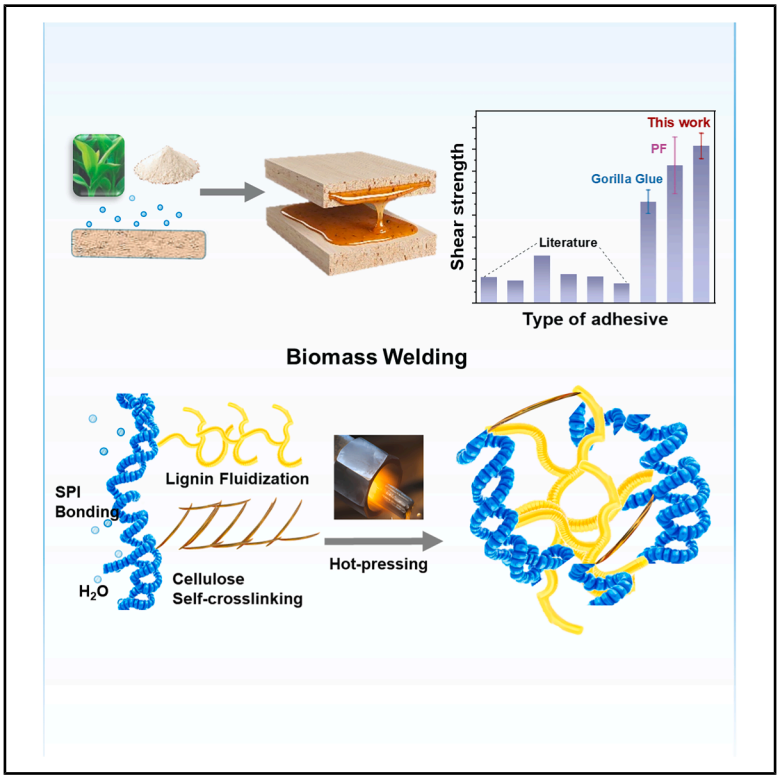

Authors

Qimin Tian, Xinyu Qiao, Guobiao Jin, ..., Hai Lin, Zirui Lou, Feng Pan

Correspondence

zrlou@pku.edu.cn (Z.L.), panfeng@pkusz.edu.cn (F.P.)

In brief

Tian et al. report a biomass welding strategy that produces ultra-strong, fully bio-based adhesives from soy protein and water. This work provides a sustainable paradigm for high-performance composites through thermal-mechanical-regulated interfacial fusion.

Highlights

- A thermal-mechanical assembly paradigm creates ultra-strong soy protein adhesive
- A mechanism involves lignin fluidization, cellulose crosslinking, and covalent bonding
- The adhesive via biomass welding requires no synthetic modifier
- The fully bio-based system exhibits closed-loop emissions and industrial viability

Tian et al., 2026, Cell Reports Physical Science 7, 103216
April 15, 2026
https://doi.org/10.1016/j.xcrp.2026.103216

CellPress

Cell Reports
Physical Science

CellPress
OPEN ACCESS

Article

Thermal-mechanical triphasic assembly enables ultra-strong soy protein adhesives via biomass welding

Qimin Tian,[1] Xinyu Qiao,[1] Guobiao Jin,[1] Xinlin Shi,[1] Lu Wang,[1] Yumeng Lan,[1] Zhaohuang Zhan,[1] Peng Du,[2] Jianyu Wang,[3] Junping Jia,[4] Xiaomin Xu,[3] Hai Lin,[1] Zirui Lou,[1,*] and Feng Pan[1,5,*]

[1]School of Advanced Materials, Peking University Shenzhen Graduate School, Shenzhen 518055, P.R. China
[2]K.H. Kuo Center for Material Characterization, Liaoning Academy of Materials, Shenyang 110000, P.R. China
[3]Institute of Materials Research, Shenzhen International Graduate School, Tsinghua University, Shenzhen 518055, P.R. China
[4]College of Materials Science and Engineering, Shenzhen University, Shenzhen 518055, P.R. China
[5]Lead contact
*Correspondence: zrlou@pku.edu.cn (Z.L.), panfeng@pkusz.edu.cn (F.P.)
https://doi.org/10.1016/j.xcrp.2026.103216

SUMMARY

The development of sustainable adhesives that combine high mechanical strength with environmental compatibility remains a challenge. Here, we report a simple strategy to fabricate ultra-strong, fully bio-based adhesives from soy protein isolate (SPI) and water. Through optimized hot pressing (160°C, 1.5 MPa, 8 min), the plywood achieves a record shear strength of 15.46 MPa, surpassing phenol-formaldehyde resins. Multi-scale characterization reveals a welding-inspired triphasic assembly mechanism: lignin fluidization (150°C) enables interfacial penetration, cellulose self-crosslinking reinforces the scaffold, and covalent C–N/C–O bonding locks SPI-wood interfaces. This approach eliminates synthetic modifiers, exhibits closed-loop emissions (primarily H_2O/CO_2), and demonstrates industrial viability. Our work addresses critical challenges in biomass composites and provides a framework for energy-controlled interfacial fusion in sustainable materials, with potential in smart materials and green engineering.

INTRODUCTION

The global adhesive industry relies heavily on petroleum-derived resins, with over 200 million tons of formaldehyde-based adhesives consumed annually, posing severe health and environmental hazards. Notably, biomass-derived adhesives,[1,2] particularly those based on plant proteins and lignin,[1–7] have emerged as promising sustainable alternatives due to their renewability, biodegradability, and low toxicity. They significantly reduce reliance on petrochemical resources, promote the recycling of waste resources, reduce the use and release of harmful chemicals (such as formaldehyde), and are in line with SDG 12, circular economies, and the principles of green chemistry. These adhesives exhibit broad applicability across multiple industries, including biomedicine,[8,9] specialized applications,[10] and circular economies of wood panels.[11] In wood composites, they serve as sustainable alternatives to formaldehyde-based resins for plywood, particleboard, and fiberboard, meeting stringent mechanical standards (e.g., EN 310 and GB/T 9846-2015) while significantly reducing volatile organic compound (VOC) emissions,[12–14] with modified soy protein variants achieving shear strengths of 2–4 MPa—comparable to commercial products.[15–17] However, their widespread industrial adoption is often hindered by limitations[18] such as poor water resistance[19,20] and unstable mechanical properties.[21] Consequently, a key research challenge lies in enhancing performance through either adhesive modification or process optimization while gaining a deeper understanding of the underlying bonding mechanisms to overcome performance bottlenecks.

Recent efforts have focused on chemical modification or nanomaterial reinforcement through molecular design, crosslinking strategies, and composite engineering to enhance performance, as bio-based adhesives rely on diverse bonding mechanisms rooted in their unique molecular structures and interactions, yet these approaches often introduce synthetic additives or complex processing steps, undermining sustainability. For instance, soy-protein-based adhesives achieve cohesion through hydrogen bonding, hydrophobic interactions, and covalent crosslinking facilitated by modifiers such as epoxy resins or polyamidoamine-epichlorohydrin.[15,16,22] The exposure of functional groups (-NH_2, -COOH, and -OH) during protein denaturation enables chemical reactions with crosslinkers, forming dense networks that enhance water resistance and mechanical strength.[23] Covalent bonding (e.g., epoxy-amine networks[23]), hydrogen bonding, and ionic interactions enhance cohesion strength, while nanomaterials (e.g., cellulose nanocrystals[9]) or bioinspired architectures (e.g., mussel-inspired catechol chemistry[24]) improve toughness and durability.

Biomass-derived adhesives—fabricated from proteins (e.g., soy and gelatin[25]), polysaccharides (e.g., starch[14,26] and chitosan[27]), and lignin[1,28,29]—offer advantages such as biodegradability and low toxicity. Among them, soy protein is promising

but hindered by poor water resistance and unstable mechanics. Previous studies relied on chemical modifications, compromising sustainability.[3–5,11,15,30–33] The raw material sources of soy protein gel can include one or more of soy protein isolate (SPI), strong gel soy protein, soybean meal (SM), soybean flour (SF), and defatted soybean flour (DSF). The preparation, testing methods, and performance of soy protein adhesives in different papers are compared (Table S1). The dry strength of the plywood they prepared is mostly between 2 and 3 MPa, and the wet strength is mostly between 1 and 2 MPa, leaving some room for improvement.

Due to the inherent trade-off between rigidity and toughness, plywood usually exhibits brittle fracture and is prone to damage and deformation defects in production applications.[34] Meanwhile, hot pressing is the most commonly used method for manufacturing artificial boards, which can expel water vapor, form a bonding interface, and solidify the adhesive. However, the synergistic effects of processing parameters, including hot-pressing temperature, duration, pressure, and pretreatment method, and their structure-activity relationships remain unclear.

Moreover, the fundamental mechanisms governing adhesion in biomass systems—particularly under thermal-mechanical processing—remain underexplored. Previous researchers of protein-based adhesives only conducted hot pressing at a relatively low temperature of 120°C[5,11,15,31] and found that the performance would significantly decline when the hot-pressing time exceeded 15 min.[35] Common pretreatment methods include prepressing (e.g., 1.2 MPa pressing for 40 min[15]) and preheating (e.g., dried for 2 h at 120°C[3]). The reasons they did not continue to increase the temperature and regulate parameters such as hot-pressing time and pressure might include excessively high temperatures easily causing carbonization of the adhesive and rapid evaporation of moisture and how, when the hot-pressing temperature was raised to 150°C, the performance gradually declined. Crucially, previous studies did not link substrate material transformations with adhesive curing reactions and did not extensively study the kinetic characteristics of the group reactions between cellulose, lignin in wood-based substrates, and soy protein.

In this work, we systematically investigate the influence of hot-pressing parameters on adhesive strength. The plywood we prepared with soy protein as the adhesive has the strongest shear strength to date we are aware of, which was obtained at a hot-pressing temperature that was previously considered unsuitable. An anomalous increase in strength observed at 160°C prompts a detailed investigation into the adhesive-substrate interactions. Inspired by metallurgical welding principles, we hypothesize that effective biomass adhesion necessitates energy-driven interfacial fusion. This leads to the proposal of a "thermo-mechanical-regulated triphasic assembly" paradigm, in which the spatiotemporal coordination of lignin flow, cellulose restructuring, and covalent bridging achieves robust adhesion, analogous to welding. Unlike conventional hydrogel adhesives relying on physical crosslinking, our system leverages thermally triggered covalent assembly akin to metallurgical joining, providing permanent interfacial fusion, which breaks through the constraints of the traditional framework and broadens the temperature and experimental parameters of the hot pressing of the soy protein adhesive. Furthermore, we also verify its practicality.

RESULTS

Thermo-mechanical optimization and ultra-strong soy protein adhesive

By making full use of the cellulose and lignin in the wooden substrate itself, the adhesive is obtained by simply mixing soy protein with water, and it is named SPIX (X is the ratio of water to SPI). By regulating hot-pressing temperature, pressure, time, and moisture, which have not been carefully studied by predecessors, attempts were made to prepare plywood with high shear strength and sustainable industrial applications (Figure 1A). The proton nuclear magnetic resonance spectrum of SPI4 shows that we have successfully prepared a soy protein adhesive (Figure S1). This adhesive is a pale yellow gel-like liquid, and its viscosity gradually decreases with the water content (Figure S2A).

The wood-based plywood (Figure S2B) was prepared by hot pressing with SPIX adhesives, named wood@SPIX (X is the ratio of water to SPI), and then tested using a universal testing machine (Figure S3). Systematic optimization revealed that a water-to-SPI ratio of 4:1 under hot pressing at 160°C, 1.5 MPa, and 8 min yielded plywood with an ultra-high shear strength of 15.46 MPa (Figures 1B–1E). This performance is 5-fold higher than conventional soy protein adhesives, setting a benchmark (Table S1).

The selection and adjustment of hot-pressing conditions and moisture content are of great significance because different hot-pressing conditions result in varying degrees of reaction between the adhesive and the substrate, and the water-mediated curing effect facilitates interfacial entanglement. Although it seems that the performance is best when the ratio is 3, the most optimal and practical ratio would be 4, as water undergoes significant evaporation under practical application conditions (Figure 1E). In addition, we conducted a principal-component analysis of the process parameters of the plywood, and the results were consistent with our experimental results (Figure S4).

Using the process from classical literature,[11,31] the shear strength can reach 5 MPa, which is consistent with reported data, with the minor differences possibly arising from variations in sample preparation techniques and processing details not fully described in the literature (Figure 1F). Using our optimal process, the maximum shear strength can reach 15.46 MPa, which is, to the best of our knowledge, the highest value among soy protein adhesives.[4,13,14,16,17,25] In addition, the performance of plywood prepared with phenolic resin (PF) using our process has also been greatly improved, but our wood@SPI4 plywood's performance still exceeds that of a classic PF adhesive under the same fabrication procedure. Besides, a comparison with the commercially available woodworking adhesive Gorilla Glue was conducted, which also demonstrated our significant superiority in shear strength performance (Figure 1G).

The shear strength is an important parameter for evaluating the performance of industrial hot-pressing wood adhesives.

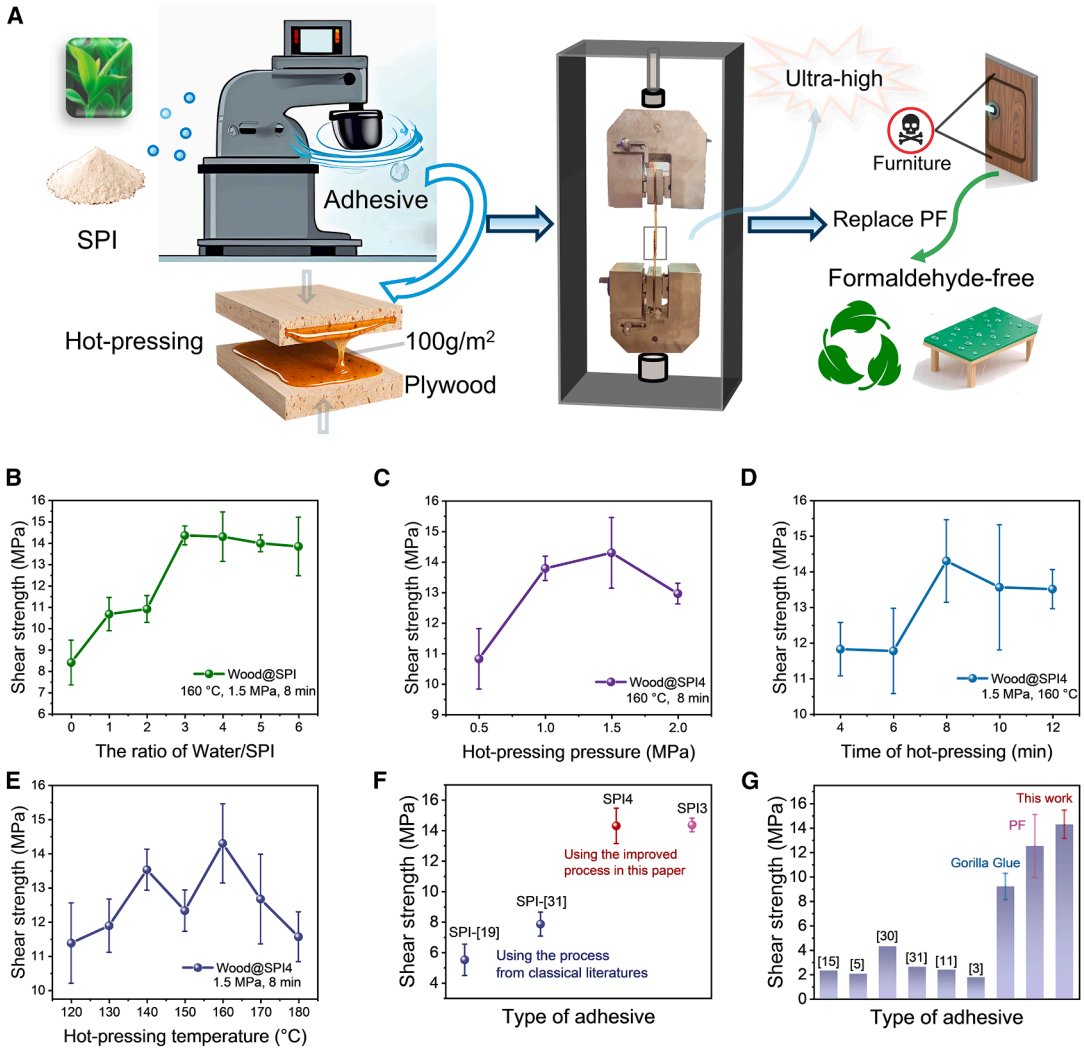

Figure 1. Process optimization and improved mechanical performance of wood@SPI plywood

(A) Schematic diagram of the preparation, standardized shear testing, and real-world application scenarios of soy protein adhesive and plywood.

(B–E) Shear strength test of wood@SPI plywood and its dependence on critical processing parameters. The variation of shear strength with the ratio of (B) water/SPI, (C) hot-pressing temperature, (D) time of hot pressing, and (E) hot-pressing pressure. Data are represented as the mean ± SE (standard error).

(F) The performance enhancement via using our improved process (160°C, 1.5 MPa, 8 min) vs. using the process from classical literature (120°C, 1 MPa). Data are represented as the mean ± SE.

(G) Benchmarking against the mechanical properties of protein adhesives from recent reported or representative works, commercial Gorilla Glue, and phenolic resin, highlighting our record strength. Data are represented as the mean ± SE.

While the tensile strength is not the focus of our attention, it is also an important parameter for evaluating general adhesives. Therefore, we designed an experiment to test the tensile strength and found that the average tensile strengths of SPI4 adhesive and Gorilla Glue were both around 4 MPa, but our adhesive has better stability due to a lower standard deviation (Figure S5).

Notably, we observed a non-monotonic strength trend with temperature: performance declined from 140°C to 150°C but recovered sharply at 160°C, indicating a previously unreported secondary curing mechanism (Figure 1E). This is an important reason why predecessors have not conducted further explorations of the hot-pressing conditions.

SPI curing dynamics and interfacial evolution

The substantial enhancement in shear strength prompted an investigation into the mechanisms underlying the performance of the SPI-based plywood. Firstly, it is necessary to understand the characteristics of SPI, such as viscosity. The prepared SPI adhesive is a pseudoplastic fluid with a shear-thinning effect, that is, it shows rigidity similar to that of a solid at low shear rates, while it exhibits fluidity similar to that of a liquid at high shear rates (Figure S6A). The pseudoplastic behavior is similar to thixotropy in solder pastes in welding, enabling gap filling during hot pressing. Actually, in order to enhance interfacial compatibility and optimize the performance of the prepared plywood, we

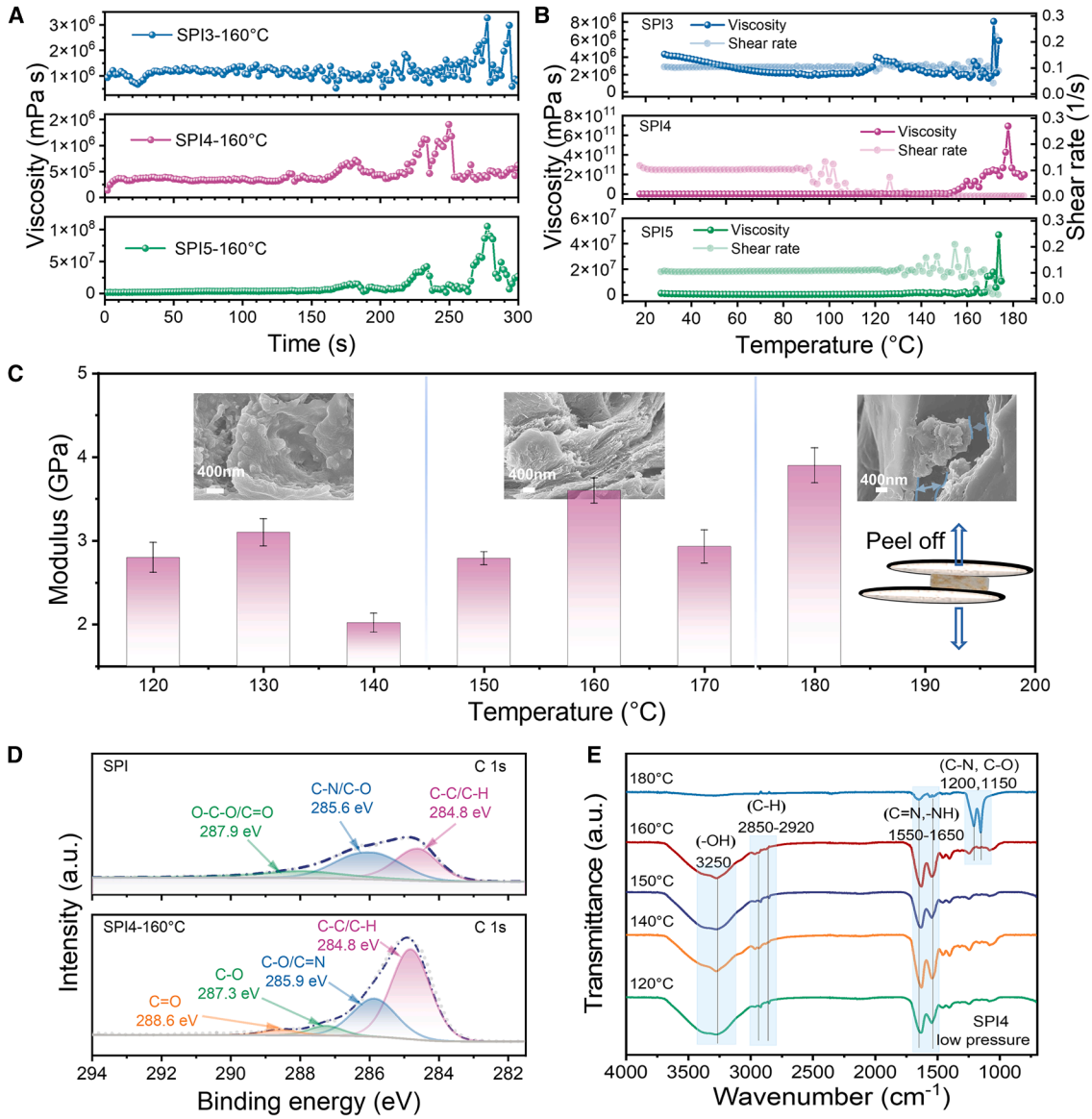

Figure 2. Molecular-scale curing dynamic properties and microscopic interfacial evolution of SPI

(A) Time-resolved viscosity profiles of adhesives with different water content ratios during pre-curing (160°C) showing multi-stage denaturation.

(B) Temperature-triggered curing thresholds for adhesives with varied hydration.

(C) Modulus mapping and SEM micrographs of SPI4 membranes demonstrating microstructural transitions including plasticity (130°C), fibration (160°C), and carbonization (180°C). Data are represented as the mean ± SE.

(D) C 1s XPS spectra of SPI and SPI4-160°C confirming covalent bond formation.

(E) Quasi-*in-situ* FTIR evidence for chemical group evolution of adhesive membranes prepared at different temperatures and a certain pressure.

implemented controlled pre-curing where protein denaturation exposes functional groups for subsequent bonding. When the adhesive is preheated at 160°C, there will be 2–3 obvious curing processes (Figure 2A). However, at 120°C, it has an insufficient degree of curing, is difficult to cure, or cures too late, and distinct curing platforms are absent (Figure S6B). This property enables the glue to better fill the gaps and form a strong bonding effect during the bonding process. From the curve of viscosity changing with temperature, it can be seen that the more moisture there is in the adhesive, the higher the temperature at which it begins to cure. SPI4 begins to cure at a temperature of around 160°C (Figure 2B). According to our research, the best pre-curing effect can be achieved by preheating SPI4 at 160°C for 3 min. Furthermore, it can be seen from the thermogravimetric (TG) curve (Figure S6C) that soy protein experiences two significant weight losses at 60°C–140°C and 280°C–340°C. The first weight loss is mainly due to water loss from the surface, which can result in exposure of surface groups, while the second weight loss may

involve protein decomposition and carbonization. Therefore, the most suitable temperature for the adhesive reaction should be within the range between them.

For the convenience of gluing and the stability of the adhesives, the absolute value of the initial zeta potential should be as large as possible to prevent the coagulation of the adhesives from affecting the final bonding effect.[36,37] On the other hand, we also hope that the adhesive has a certain particle size that can form a certain aggregate structure on the surface of the substrate, enhancing the resilience of subsequently cured adhesive layers. The absolute values of the average zeta potential of the three SPI adhesives with different water contents are all less than 5 (Figure S6D), indicating that they are all prone to coagulation. The particle sizes of the three adhesives with different water contents all reached the micrometer level, among which SPI4 produced the largest aggregates under the action of water (Figure S6E).

Isolation of SPI adhesive layer

Next, to gain deeper insights into the underlying mechanisms responsible for the superior performance, it is crucial to obtain comprehensive information about the adhesive layer. Former researchers directly conducted the Fourier transform infrared (FTIR) test on the broken plywood, but since the connection between the adhesive and the substrate has already broken, some chemical bonds are likely to have been opened, and in the meantime, the flatness of the fracture surface and the uneven exposure of the interface would have a significant adverse impact on the test, thus making it impossible to obtain truly effective information. Ideally, direct characterization of the adhesive layer through microscopic analysis would significantly enhance our understanding of its bonding mechanisms. However, in the case of adhesive-coated wood veneers subjected to hot pressing, the adhesive layer becomes firmly bonded between the two substrates, making physical extraction impractical. Conventional destructive separation methods inevitably compromise the structural integrity of the bonding layer. Consequently, direct characterization of the adhesive layer within the plywood is critically challenging.

Our initial attempts using polytetrafluoroethylene (PTFE) substrates revealed poor adhesion and good separability, suggesting a route to isolate the adhesive layer. However, the hydrophobicity of PTFE differs significantly from that of wood, potentially altering moisture distribution and reaction pathways. To better mimic the actual bonding interface while enabling membrane extraction, a method was developed incorporating hydrophilic PTFE filter membranes between wood veneers (Figures S7 and S2C). This approach allowed controlled moisture transport while facilitating the retrieval of intact adhesive membranes for characterization.

Microstructural transitions of the SPI adhesive layer and two hypotheses

It can be found through electron microscopy combined with touch and visual observation that when the hot-pressing temperature is relatively low (130°C), the adhesive layer is relatively soft, similar to the characteristics of polymers. However, when the temperature is 160°C, there is a tendency for solidification and fibrosis of the adhesive layer, and it reaches a relatively stable state, which can be considered to be more compatible with the substrate. But when the temperature is too high (180°C), the adhesive layer is over-cured or even carbonized, resulting in a decrease in the final bonding performance (Figure 2C).

The atomic force microscopy (AFM) and modulus tests of the adhesive membrane show that the texture of the adhesive membrane at 160°C is relatively uniform, and the average modulus reaches more than 3.5 GPa (Figure 2C). Particularly, 140°C is precisely the critical point at which the adhesive strength reaches its peak for the first time and the modulus of the adhesive membrane is the lowest. This might indicate that the first bonding reaction is about to reach its peak, while the secondary reaction of the substrate is a side reaction at this time and has not yet fully occurred; therefore, 140°C is not the real optimal hot-pressing temperature, which may have been mistaken by previous researchers. The relevant data for other temperatures can be seen in Figure S8.

In the UV spectrum, it was observed that at 160°C, the adhesive membrane exhibited an absorption peak in the range of 240–250 nm (Figure S9). This phenomenon could be attributed to the protonation of electrons in the n-orbitals of nitrogen (N) or oxygen (O) atoms on the SPI by the protic solvent water. Protonation of these heteroatoms enhances their electron-withdrawing effect, thereby attracting the electrons in the n-orbitals closer to the nucleus and reducing their energy levels.[38] The gyration radius of SPI through small-angle X-ray scattering (SAXS) is 7.06 nm (Figure S10). During the curing process of the powder soy protein adhesive, the unfolding of proteins reduces intramolecular bulk density. However, as the hot-pressing temperature increases, the intramolecular bulk density of the protein film gradually increases, and the average size of the molecules also increases.[39]

To analyze the composition of chemical groups and elements on the surface of soy protein and the adhesive film, in order to determine the group changes during the curing process of the adhesive, X-ray photoelectron spectroscopy (XPS) characterization with spectral deconvolution was performed. According to the XPS survey spectrum (Figure S11), the proportions of carbon, nitrogen, and oxygen elements in SPI are 71.6%, 13.2%, and 15.2%, respectively.[40] After SPI was heated and solidified with water, the XPS peak of SPI shifted toward a lower binding energy. Moreover, it was found from the C 1s spectra (Figure 2D) that the C–N and C=O bonds partially transformed into C–C bonds,[41,42] and the elemental proportions of carbon, nitrogen, and oxygen changed to 73.5%, 6.7%, and 19.8%, respectively. This is because the oxygen atoms in water carry lone pairs of electrons and can act as nucleophiles to provide electron pairs. This causes a reduction reaction in SPI, and there is a hydrogen-bond interaction.[43]

Infrared spectroscopy tests further confirmed the group analysis results of XPS. SPI contains chemical bonds such as C=O, C–N, N–H, and C–C (Figure S12), and C=N is produced at hot-pressing temperatures ranging from 120°C to 160°C. But it is worth noting that the FTIR spectra of the adhesive membranes show that, at 180°C, the C=N and N–H bonds are transformed into C–N and C–O bonds, respectively (Figure 2E). Two hypotheses could explain these observations. Hypothesis 1 is that

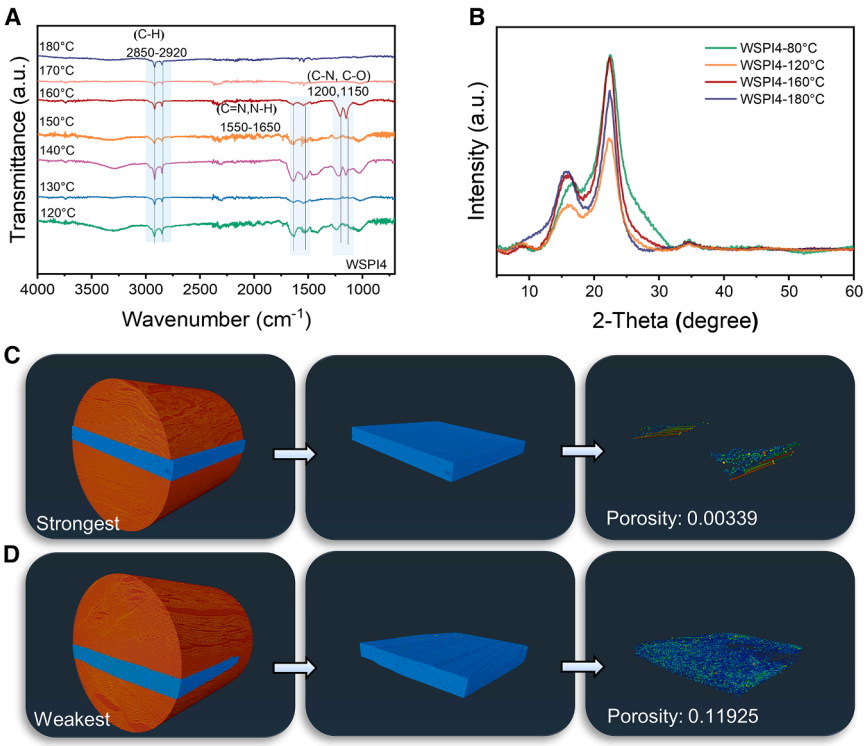

Figure 3. Bonding principle between adhesives and substrates revealed through multi-technique and cross-scale characterization

(A) Quasi-*in-situ* FTIR of WSPI4 membranes prepared at different temperatures showing bond formation thresholds.

(B) HXRD patterns of WSPI4 membranes at different temperatures tracking cellulose/lignin reorganization during thermal curing.

(C and D) Micro-CT 3D reconstructions contrasting adhesive morphology in (C) strongest-strength and (D) worst-strength specimens. Scale: 1 μm. The brownish-yellow area is the reconstructed wood, and the blue area is the adhesive layer area confirmed by manual positioning.

excessive temperature leads to adverse side reactions such as carbonization and breakage. Hypothesis 2 is that the formation of new chemical bonds represents a beneficial secondary reaction but that its effectiveness depends on the availability of reactive sites in the substrate, which may be depleted at higher temperatures.

The two hypotheses and the above research indicate that the interaction between substances in the substrate and the adhesive itself would potentially have a significant impact on the final performance. To verify which hypothesis is more reasonable, after conducting microscopic characterization of the adhesive membranes, we considered whether we could understand the bonding mechanism between wood and the adhesive more accurately. Once again, we conducted an experiment by mixing the powder of the wooden substrate with SPI and preparing the adhesive WSPI4 (the abbreviation of the adhesive obtained by mixing wood powder with SPI4 adhesive) according to the same solid-liquid ratio. In this way, we could expose sufficient wood-adhesive interfaces under real temperature and pressure to simultaneously track interfacial interactions between SPI and wood under curing conditions.

Wood-adhesive interfacial bonding mechanism

From the FTIR spectrum of WSPI4, we found that it was precisely at 160°C that new chemical bonds were formed (Figure 3A) and the groups of the adhesive gradually exposed after preheating (Figure S13A). Therefore, the interfacial analysis supports hypothesis 2, as chemical bond formation coincided with optimal performance at 160°C. The simultaneous input of pressure and thermal energy can cause substances in the adhesive and the substrate to react simultaneously, and a secondary adhesive reaction can be induced, forming a larger and more stable crosslinked network. Under the simultaneous action of heat and pressure, it may lead to the secondary reaction occurring at a lower temperature (160°C) with a more controllable process window. When the temperature rises to 180°C, the adhesive layer undergoes excessive carbonization, which instead weakens the chemical connection between the adhesive layer and the substrate, resulting in a decline in performance (Figures 3A and S2D–S2F).

The SPI itself begins to transform at 140°C under pressure and starts to interact with cellulose and lignin above 150°C. At 150°C, lignin began to flow,[29,44] causing the adhesive performance to decline first (Figure 1B). The effect of lignin plasticization, once it reaches temperatures above its glass transition temperature, and the consequent migration effects have been thoroughly reviewed.[45] This further corroborates hypothesis 2. The high-power X-ray diffraction (HXRD) of the WSPI4 adhesive membrane also indicates that the peak area is the largest at 160°C (Figure 3B). The peak narrowing at 22° indicates enhanced cellulose crystallinity, while peak shifts suggest lattice reorganization during bonding, which also proves that the cellulose and lignin in the substrate are most closely combined with the adhesive, as 14°, 22°, and 35° are the crystallization peaks of lignocellulose. The TG curve (Figure S6C) indicates that the adhesive rapidly loses water at over 100°C and reaches a relatively stable plateau at approximately 150°C–160°C. Studies have shown that at 150°C, lignin melts and adheres to the residue (cellulose-rich matrix), and the retention rate of cellulose drops sharply.[46] At 160°C, the groups of both were fully exposed, accompanied by the self-crosslinking of cellulose.[47] Lignin fluidization (150°C) mimics solder melting, while cellulose crystallization forms weld-like scaffolds. To further demonstrate that lignin flows at a certain temperature and reacts with the adhesive, we conducted a differential scanning calorimetry (DSC) cycle test and found that there was no obvious peak in SPI, wood, and cellulose (Figure S14A), but there was a small reaction peak of WSPI4 near 130°C in the first cycle (Figure S14B).

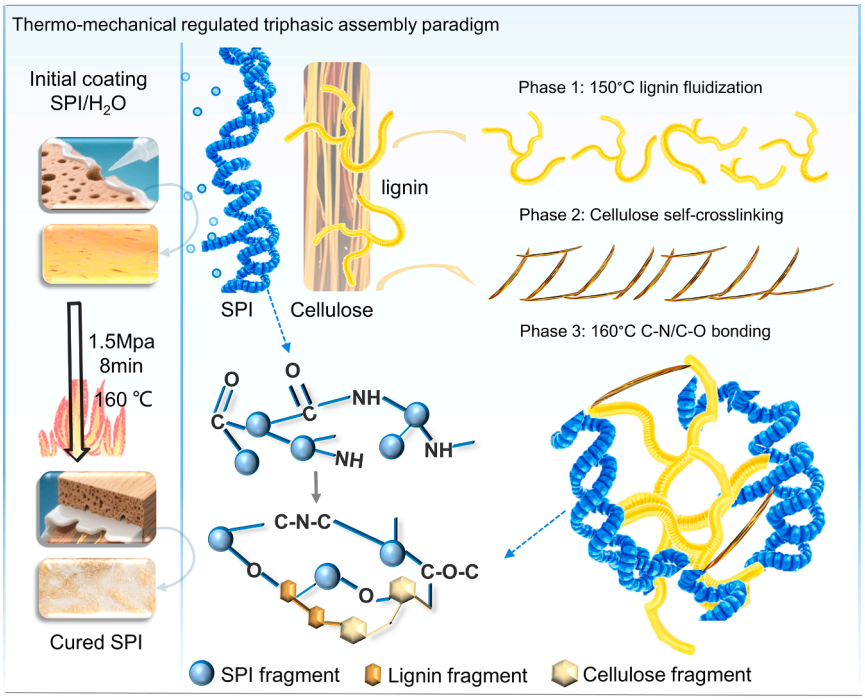

Figure 4. Welding-inspired thermo-mechanical-regulated triphasic assembly paradigm mechanism for biomimetic adhesion with wooden substrate

Phases 1–3 depict an interfacial fusion process analogous to soldering (150°C: lignin fluidization = solder melting; 160°C: C–N/C–O bonding = metallurgical joint formation). Phase 1: lignin fluidity-driven interfacial penetration (150°C). Phase 2: cellulose self-crosslinking for structural reinforcement. Phase 3: covalent bonding (C–N/C–O) locking SPI-wood interfaces (160°C).

To eliminate the influence of cellulose in wood, we mixed cellulose with soy protein and kept the moisture content consistent to prepare CSPI4 (the abbreviation of the adhesive obtained by mixing cellulose with SPI4 adhesive) and found that there was no obvious peak (Figure S14C), which further confirmed hypothesis 2.

Mesoscale characterization via micro-CT

To analyze the bonding mechanism from the mesoscopic scale and characterize the plywood more non-destructively, we conducted microcomputed tomography (micro-CT) tests and found that samples with excellent performance have significant differences in the distribution of adhesives and the number of holes and cracks compared with the samples with poor performance (Videos S1 and S2). We then carried out 3D reconstruction based on the data from micro-CT (Figures 3C and 3D). We completed the large-scale 3D reconstruction of the substrate and plywood and extracted the reconstruction of the adhesive layer and those of the holes and throat channels of the adhesive layer. It was found that the plywood with good performance has a relatively regular and dense adhesive layer with few holes, while the plywood with poor performance has an irregular adhesive layer with many holes. The porosity of the adhesive layer of different plywood demonstrates an inverse correlation with mechanical performance. When we change the base material from wood to bamboo, we also reach the same conclusion (Figure S15). This indicates that high-performance plywood has fewer failure sites at the mesoscopic level. Low-porosity adhesive layers (<1%) resemble defect-free weld seams.

Welding-inspired thermo-regulated triphasic assembly

Based on the above research and characterizations, the welding-inspired thermo-regulated triphasic assembly in lignocellulose-protein systems between the substrate and the adhesive layer is proposed. Just as welding transforms bulk metal integration through controlled thermal input, ideal wood-adhesive interfaces demand spatiotemporal coordination of lignin flow, cellulose restructuring, and covalent bridging. Under pressure, a second chemical reaction occurs among lignin, cellulose, and SPI, forming new chemical bonds that tightly connect the two substrates together[42,48] (Figure 4). Cellulose microfibrils undergo structural densification through hydrogen-bond reorganization, while mobile lignin phases establish covalent linkages (C–N/C–O) with exposed protein functionalities, and the water-mediated curing effect facilitates interfacial entanglement across multiple length scales. Water plays an important role in the formation of hydrogen-bond networks in the early stage, but the formed covalent bonds between the adhesive and the substrate are stronger than those in previous traditional work. The reaction time is also an important influencing factor (Figure S13B). The reaction can be completed in exactly 8 min, but if the time is too long, carbonization or bond re-breaking may occur, and if it is too short, the reaction cannot be completed. Additionally, the construction of molecular-scale adhesive networks enables the bonding layer to have relatively regular and dense pores at the mesoscopic scale, resulting in fewer failure sites as a whole and ultimately demonstrating strong bonding performance at the macroscopic level. This paradigm can be extended to various biomimetic adhesions with wooden substrates.

The evolution process of the underlying chemical functional groups in the thermo-mechanical-regulated triphasic assembly paradigm can be illustrated (Figure S16). The lignin-carbohydrate complex (LCC) in wood has groups such as C=C, C=O, and C–O, which undergo fracture and separation during hot pressing. At 150°C, lignin flows, and cellulose self-crosslinks. Moreover, after the primary reaction of soy protein curing, the peptide bonds transform into C=N bonds, and a secondary reaction occurs at 160°C to produce C–N and C–O single bonds. The existence of SPI participates in and promotes the reconstruction of mesh structures similar to the LCC. The phenomenon of a secondary improvement in performance can also be explained here. The formation of new chemical bonds is a secondary adhesive

reaction, which should be conducive to expanding the crosslinked network and enhancing the adhesive strength, but if the temperature is too high, substances in the substrate, such as cellulose and lignin, complete the reaction and lose their adhesive sites. At this moment, they can no longer react with the soy protein, resulting in failure of secondary bonding, instead causing a decline in performance. Therefore, if the adhesive and the substrate can react simultaneously, the strongest performance can be achieved.

To sum up, mechanistic studies unveil a welding-inspired thermo-regulated triphasic assembly paradigm, where temperature-programmed interfacial fusion mirrors metal joining: (1) lignin fluidization (150°C) enables wood-adhesive interpenetration analogous to solder melting, (2) cellulose self-crosslinking forms load-bearing scaffolds resembling weld seams, and (3) covalent C–N/C–O bonding locks interfaces such as metallurgical bonding in welding.

The mechanistic effects of temperature on SPI adhesion to wood[49] and the interfacial interactions between SPI and cellulose[50] and lignin[51] have been studied by former researchers, but none of them considered linking these three elements together. In this work, we integrate these aspects to propose a triphasic assembly mechanism and verify it through experiments and characterization methods.

However, due to the complexity of the biomass system, it is difficult to directly determine the specific structure transformation and chemical activity of each component when energies, including heat and pressure, are input. Therefore, we acknowledge that the current mechanism's limitations mainly lie in the lack of sufficient direct evidence regarding the specific chemical pathway.

In the future, to further elucidate the mechanism, we expect that more non-destructive characterizations, such as micro-CT and *in situ* hot-pressing spectrum testing, can be discovered and carefully designed. To expand the thermo-mechanical-regulated triphasic assembly paradigm mechanism of this paper, for any "S+A+S" (substrate, adhesive, substrate) sandwich-type composite structure, it is possible to design it through this framework, fully utilizing the multiple reactions between the base and the intermediate adhesive layer to maximize the mechanical performance. Therefore, here, we draw inspiration from metallurgical welding to propose a thermo-mechanical-regulated triphasic assembly paradigm that leverages intrinsic biomaterial properties without external modifiers. By precisely controlling temperature, pressure, and hydration, we achieve exceptional adhesion strength coupled with high environmental resilience. This work not only addresses a critical sustainability challenge but also provides a foundational framework for energy-controlled interfacial fusion in biomass composites.

Environmental resilience and application demos

After clarifying the bonding mechanism, we conducted research and analysis on the practicability, water resistance, and universality of SPI adhesives. The contact angle test shows that the adhesive membrane has certain water resistance and that, as the hot-pressing temperature rises, the water resistance of the adhesive membrane will gradually improve. (Figure 5A). TG-mass spectrometry (TG-MS) proved that high-temperature heating of WSPI4 does not produce toxic gases; only water and carbon dioxide are produced, and the gas production is relatively low (Figure 5B). Therefore, our plywood fully complies with the standard GB/T39600-2021ENF grade, meaning that the formaldehyde emission is $\leq$0.025 mg/L. It should be pointed out that the ENF-level environmental protection standard is one of the most stringent environmental protection standards at present. We tested a crane and a cart with wood@SPI4 plywood in heavy rain. There was no problem at all in lifting a 70 kg person and pulling a 2-ton vehicle (Figures 5C and 5D; Video S3). The energy-controlled gelation mechanism provides design principles beyond adhesives, potentially applicable to bio-composites, degradable packaging, and wooden buildings. With the SPI4 adhesive and the process in this work, various products can be independently designed and formed in a single hot-pressing step. The products we design have potential application value in the future as wooden building foundations, wooden walkways, drainage channels, plywood, etc. (Figure 5E; Video S4).

We also verify the strength of our plywood in some extreme scenarios. After soaking the plywood in water for more than 24 h (Figure S17), its shear strength still remained above 3 MPa (Figure 5F), though there is a significant performance degradation compared to dry strength; our performance still has an advantage compared to the former working of the same type of soy protein adhesives (Table S1). The mass water absorption rate of the adhesive membrane was less than 30% and even nearly 10% when the hot-pressing temperature was 180°C (Figure S18). Additionally, we tested the shear strength of wood@SPI4 prepared with different hot-pressing times after 24 h of immersion in water (Figure S19). When we extend the hot-pressing time to 10 min, the shear strength of the plywood soaked in water for 24 h approaches 5.4 Mpa, which is similar to the water resistance of commercial PF (5.5 Mpa). The dry shear strength of wood@SPI4 remains unchanged after 1 year indoors, which proves the long-term consistency of indoor performance. In outdoor rainy and potentially bacterial environments, there may be differences in performance, prompting us to conduct extreme weather resistance tests on plywood (Figure S20). As seen in the photos, there is no obvious mold on the surface or in the cross-section, and the results of the performance test show that our adhesive still has a shear strength above 3 MPa (3.51 ± 0.11 MPa for 40 days) after being placed under extreme conditions for several days (Figure 5G), which is also better than other soy protein adhesives (Table S1).

While real-world demonstrations (e.g., cart pulling) illustrate potential applicability, we acknowledge that controlled laboratory tests are the standard for rigorous performance validation. The data presented on wet shear strength after 24-h immersion (Figure 5F) and long-term stability under various conditions (Figure 5G) provide quantitative measures of environmental resilience. Future work will include more standardized accelerated aging tests to further quantify durability.

Since the performance of wood-based plywood is excellent, we also tested it using various substrates. For instance, when using bamboo as the substrate, SPI4 also performed well, but it was slightly worse than that of the wood base. Bamboo has denser fiber bundles, and the transformation of lignocellulose

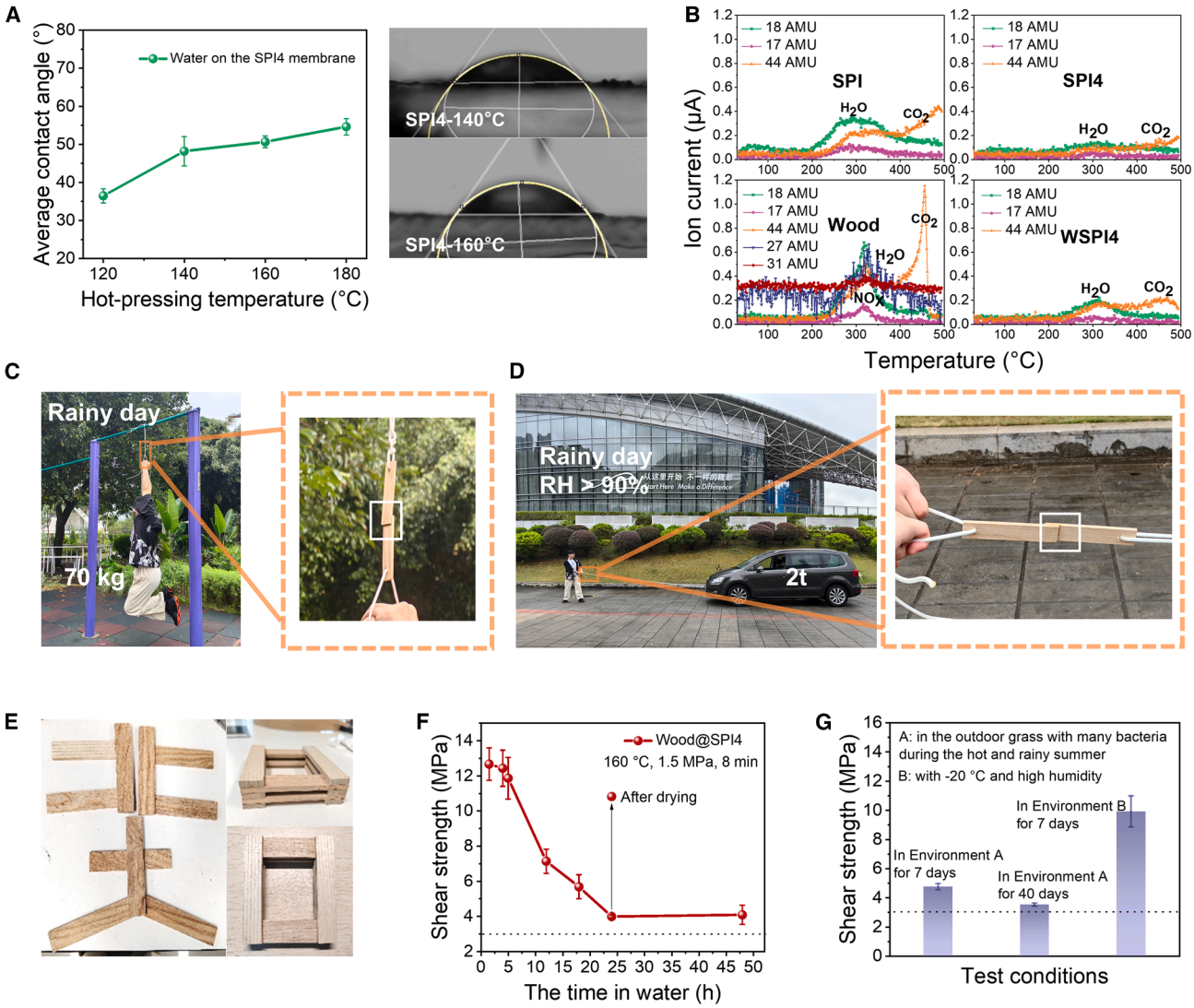

Figure 5. Environmental resilience and practical applications of SPI4 adhesive

(A) Water contact angles of adhesive membranes prepared at different temperatures. Data are represented as the mean ± SE.

(B) TG-MS profiles of SPI, SPI4, ash wood, and WSPI4 confirming non-toxic decomposition products.

(C and D) Real-world validation: wood@SPI4 plywood (only 3 cm^2 bonding area) (C) lifting 70 kg and (D) towing a 2-ton vehicle under rainy-day conditions.

(E) Diverse products using SPI4 adhesive and hot pressing in one step, demonstrating design flexibility.

(F) The mass water absorption rate of WSPI4 membranes obtained at different hot-pressing temperatures. Data are represented as the mean ± SE.

(G) Shear strength tests under extreme conditions such as low/high temperature, high humidity, heavy rain, and potential microbial attack. Data are represented as the mean ± SE.

at high temperatures may be more difficult. At the microscopic scale, the intermolecular bonds are not as tight; at the mesoscopic scale, there is anisotropy, with good mechanical properties along the axial direction but poor adhesion due to smoothness and flatness, while the transverse direction is relatively rough and suitable for adhesion but has poor mechanical properties.[52,53] Additionally, the surface of the bamboo substrate is relatively flat and has poor wettability, which might also be a reason for it. In the future, we can conduct more in-depth comparative studies on different substrates. Bamboo@SPI4 plywood based on MOSO bamboo still had good shear strength (Figure S21), demonstrating that our SPI adhesive has an excellent bonding effect on bamboo-wood substrates and attesting to its broad applicability on lignocellulosic surfaces.

DISCUSSION

This study demonstrates an alternative approach to bioadhesive design that emphasizes physical field control over chemical modification. The triphasic assembly mechanism, analogous to metallurgical bonding, offers a framework for understanding interfacial fusion in biomass systems. This strategy achieved high

mechanical performance while maintaining full recyclability and non-toxic decomposition. The identification of a secondary reaction mechanism between the adhesive and substrate highlights the importance of thermal-mechanical synergy, an aspect potentially overlooked in previous studies due to concerns about premature carbonization. Our methodology—combining multiscale characterization with particular membrane extraction—provides an avenue for studying buried interfaces in composite materials.

The optimized protocol involving vortex-mixed SPI/water systems under strategic hot-pressing conditions resulted in a shear strength of 15.46 MPa for the plywood, which exceeds the performance of conventional PFs and previously reported soy protein adhesives. We pioneer a welding-inspired thermo-mechanical-regulated triphasic assembly paradigm where (1) mobile lignin phases enable interfacial penetration, (2) cellulose microfibrils form load-bearing networks and undergo structural densification through hydrogen-bond reorganization, and (3) covalent linkages (C–N/C–O) lock protein-substrate interfaces. Mechanistic investigations reveal a hierarchical bonding paradigm where thermally activated molecular rearrangement drives synergistic interactions. The water-mediated curing effect facilitates interfacial entanglement across multiple length scales. This work establishes a biomass welding framework in which thermal-mechanical inputs drive interfacial fusion across scales. The triphasic assembly—mirroring the melting-penetration-solidification sequence in welding—transcends traditional "adhesive-coating" logic, instead creating monolithic wood-protein hybrids with covalent interfaces. This strategy not only addresses strength limitations but also aligns with circular economy principles, enabling applications in degradable packaging and smart composites.

The identified paradigm overcomes the long-standing performance limitations observed in bioadhesives. Practical evaluations confirm exceptional environmental resilience, including sustained mechanical integrity during 24-h water immersion (3 MPa retention) and extreme load-bearing capacity under real-world conditions. This work establishes a fundamental framework for biomaterial engineering through energy-state manipulation, where controlled thermal inputs activate inherent molecular recognition between plant components. Our findings suggest that protein-based adhesion mechanisms may reflect conserved principles of biological interfacial engineering, providing potential design principles for bioinspired structural materials.

METHODS

Materials

All commercial chemicals were analytical reagents and used without further purification. SPI (biological reagent, BR) was purchased from Shanghai Yuanye Bio-Technology. The Gorilla Glue used in this article is Gorilla Wood Glue, made in Cincinnati, Ohio, USA.

Preparation of SPI adhesives

A certain amount of SPI was weighed and mixed with deionized water in a certain ratio (water:SPI = 0, 1, 2, 3, 4, 5, and 6) in a vortex oscillator at 2,000 rpm for 10 min, followed by ultrasonic treatment for 3 min to prepare SPI gel-like liquids. These were named SPI0–SPI6 according to the ratio of water to SPI. The next part illustrates the detailed process and parameters of the preparation of plywood using the SPI adhesives prepared above.

Preparation of wood@SPI plywood

The prepared gel-like liquids were applied to the substrates (wood and bamboo) at a glue application rate of 100 g/m^2. Since the plywood we prepared for testing has an adhesion area of only 3 cm^2, the amount of glue applied was only 0.03 g (solid content). They were preheated for 3 min at a certain temperature (120°C–180°C), then hot pressed at the same temperature and under a certain pressure (0.5–2 MPa) for a certain time (4–12 min), and naturally depressurized and cooled for 3 min to obtain a series of boards. The preheating and hot-pressing processes were both accomplished in an R32022021 QIXING Vacuum Mini Hot Press. The power switch was turned on, the temperatures of both the upper and lower plates of the hot press were set to a certain value (e.g., 160°C), and then the heating switch was turned on. When the set temperature was reached, the glued wood sandwiched between two layers of stainless-steel plates was placed between the heating plates, and pressure to a specific value (such as 1.5MPa) was applied. The heating element utilizes infrared, far-infrared carbon fiber stainless-steel high-temperature-resistant wire, which is embedded and installed. The temperature controller adopts imported temperature control units and relays to realize the proportional-integral-derivative (PID)) control mode, which can precisely control the temperature.

Bonding strength evaluation

The shear strength and tensile strength of the plywood were tested using a universal testing machine at a rate of 5 mm/min as part of the system project "plastics-determination of tensile properties." Because the maximum tensile force limit of the machine is 5,000 N, the adhesion area of plywood is set at 3 or 1 cm^2. The maximum force (F) applied to joints before failure was recorded. The resulting shear strength was calculated by dividing F by the joint overlap area (A). The number of test samples for each data point is at least 10, ensuring that the fracture of each sample is caused by the adhesive layer rather than the substrate and discarding any outliers that deviate from the average value by more than 3 MPa.

Molecular-scale and microscopic characterization

Laser particle size analyzer

The SPIX (X = 3, 4, and 5) was diluted in equal proportion, and the particle size distribution and zeta potential were tested on the Zetasizer Nano ZS90. Scattered lights of different angles were passed through a Fourier lens and formed halos of different radii on the focal plane, which contained information about the size and distribution of the particles.

Rheological testing

The rotational rheometer measurement system (Haake MARS II) came into contact with the SPI adhesives and applied a load to measure torque in steady-state mode. Physical quantities (torque and rotational speed) were converted into rheological parameters using a fixture coefficient. By controlling parameters

such as temperature (25°C–180°C) and shear rate (0.1–10 1/s), the viscosity of the adhesive can be measured *in situ* as it changes over time or temperature. The mass of the samples we used for testing was 0.6 g (solid content), and SPI adhesives were prepared by adding water at solid-liquid ratios of 1:3, 1:4, and 1:5, respectively.

Scanning electron microscopy imaging

The cross-sections of the broken plywood, adhesive membranes, and wood-adhesive interfaces were analyzed via scanning electron microscopy (SEM; ZEISS SUPRA 55) to observe the softness and hardness states and cross-sectional states of the adhesive membrane at different temperatures.

FTIR

Based on the infrared spectra (Thermo Scientific Nicolet iS50) of SPI4 adhesive membranes, WSPI4 membranes, wood chips, adhesives, and wood@adhesives, it is possible to predict which groups may have interacted and which chemical bonds are involved in the adhesion process. Additionally, by analyzing the changes in the infrared spectra of the adhesives at different times and temperatures, *in situ* infrared tests can be conducted to analyze the changes in groups during the adhesion process.

HXRD

WSPI4 membranes were placed on single-crystal silicon wafers with low angles and no peaks. The crystallinity changes of cellulose and lignin in WSPI4 were analyzed by HXRD (Bruker D8 Discover), which reflected the reaction between the film and the wood substrate from the side.

DSC

Under an air atmosphere, raw materials such as WSPI4, CSPI4, wood, SPI, and cellulose were raised from 20°C to 200°C at a rate of 5°C/min, with a focus on observing the heat absorption and release within the range of 120°C–180°C to verify the flow and reaction of lignin, with DSC1 (METTLER TOLEDO).

XPS

Surface chemistries of the samples were examined with ESCALAB 250× (Thermo Fisher Scientific). Several elements of bond breaking, including the C spectrum, N spectrum, and O spectrum, were identified via XPS. The membranes were tested after etching for more than 10 s.

SAXS

The distance from the sample to the detector was set at 640 mm. The rotation radius was obtained by fitting the low-Q region data through Guinier analysis, and the molecular stacking degree and average size of the sample were analyzed with Anton Paar SAXSpoint 5.0.

AFM

By detecting the extremely weak interatomic interaction force between the adhesive surface and a micro-force sensitive element with Bruker MultiMode 8 in mapping mode, the surface structure and properties of the adhesive can be studied, and surface morphology and roughness information can be obtained at nanometer resolution.

UV-vis spectrophotometry

Using a special glass with almost no absorption of far-UV light as the substrate, the SPI adhesive was coated on the substrate, and the absorption spectrum was tested with a UV spectrophotometer (UV-2450).

Mesoscopic characterization and practical environmental protection verification

Micro-CT and reconstruction

X-rays were used to penetrate the material with Xradia 620 Versa, and the attenuation of the X-rays after passing through the strongest plywood and the worst plywood in this work was detected to construct an internal structure image of the material. This non-destructive method characterizes the internal structure, cracks, defects, and the distribution of fillers and matrix of the adhesive and substrate. The 3D reconstruction of plywood was accomplished using Avizo 3D software. The main steps included importing micro-CT images and reducing noise, marking the adhesive layer interface, finding isolated pores and connected pores, sieving analysis, calculating porosity, pore diameter and larynx, and 3D rendering.

TG analysis and TG-MS

By measuring the mass change of materials at different temperatures (30°C–600°C, air atmosphere, heating rate of 5°C/min) with a simultaneous thermal analyzer (METTLER TOLEDO), the thermal stability and decomposition temperature of the binder, as well as other thermal performance parameters, can be understood. At a temperature range of 30°C–500°C, a heating rate of 5°C/min, an experimental atmosphere of high-purity air, and a mass spectrometry mass number range of 1–300 amu, TG-MS tests of SPI powder, SPI adhesive, ash wood powder, and WSPI4 suspension were conducted by Thermo plus EVO2.

Contact angle meter

By placing water droplets on the surface of the SPI membrane and measuring the contact angle between the droplets and the membrane surface using Ossila L2004A1, the interaction force between water and the membrane surface can be determined, thereby understanding the water resistance of the membrane.

RESOURCE AVAILABILITY

Lead contact

Requests for further information and resources should be directed to and will be fulfilled by the lead contact, Feng Pan (panfeng@pkusz.edu.cn).

Materials availability

Adhesives generated in this study will be made available on request, but we may require a payment and/or a completed materials transfer agreement if there is potential for commercial application.

Data and code availability

- The bonding strength data have been deposited at Science Data Bank and are publicly available as of the date of publication at Science Data Bank: https://doi.org/10.57760/sciencedb.37160.
- All other data needed to evaluate the conclusions in the paper are present in the paper and supplemental information.
- This paper does not report original code.
- Any additional information required to reanalyze the data reported in this paper is available from the lead contact upon request.

ACKNOWLEDGMENTS

This work was financially supported by the Guangdong Key Laboratory of Design and Calculation of New Energy Materials (no. 2017B030301013); the National Center for International Research of Power Batteries and Materials

(no. 2015B01015); the Shenzhen Key Laboratory of New Energy Resources Genome Preparation and Testing (no. SYSPG20241211173440007); and the Major Science and Technology Infrastructure Project of Material Genome Big-science Facilities Platform supported by the Municipal Development and Reform Commission of Shenzhen, National Natural Science Foundation of China (grant no. 92472206).

AUTHOR CONTRIBUTIONS

Q.T. carried out all experiments and most tests, conceived the mechanism, created all of the figures, and wrote the manuscript. X.Q. provided ideas for figure creation. G.J. conceived the concept of welding. X.S. performed the SEM experiments. L.W. provided ideas for 3D reconstruction. Y.L. participated in the experimental design. Z.Z. performed the DSC/TGA experiments. P.D. performed the micro-CT experiments. J.W. performed the AFM experiments. J.J. performed the SAXS experiments. X.X. and H.L. provided test platform support. Z.L. and F.P. provided revision suggestions and support.

DECLARATION OF INTERESTS

The authors declare no conflicts of interest.

SUPPLEMENTAL INFORMATION

Supplemental information can be found online at https://doi.org/10.1016/j.xcrp.2026.103216.

Received: January 8, 2026
Revised: February 4, 2026
Accepted: February 27, 2026
Published: March 30, 2026

REFERENCES

1. Yang, G., Gong, Z., Luo, X., Chen, L., and Shuai, L. (2023). Bonding wood with uncondensed lignins as adhesives. Nature *621*, 511–515.
2. Westerman, C.R., Mcgill, B.C., and Wilker, J.J. (2023). Sustainably sourced components to generate high-strength adhesives. Nature *621*, 306–311.
3. Huang, X., Chen, Y., Lin, X., Li, J., and Gao, Q. (2023). A strong soy protein-based adhesive with excellent water retention. Chem. Eng. J. *472*, 145037.
4. Xu, Y., Han, Y., Li, Y., Li, J., Li, J., and Gao, Q. (2022). Preparation of a strong, mildew-resistant, and flame-retardant biomimetic multifunctional soy protein adhesive via the construction of an organic-inorganic hybrid multiple-bonding structure. Chem. Eng. J. *437*, 135437.
5. Li, Z., Niu, W., Cai, L., Li, J., Chen, H., and Gao, Q. (2024). Performance of eco-friendly soy protein adhesive reinforced by aldehyde sodium alginate. Int. J. Adhes. Adhes. *131*, 103649.
6. Zhu, Z., Li, X., Li, X., Li, J., Sun, W., Gao, Q., and Zhang, Y. (2024). Pulp cellulose-based core–sheath structure based on hyperbranched grafting strategy for development of reinforced soybean adhesive. Int. J. Biol. Macromol. *260*, 129520.
7. Zhang, X., Zhang, X., Cai, L., Li, J., Song, P., Li, J., and Gao, Q. (2024). Strong and antistatic biomass adhesive for wood-based composites with electrostatic discharge protection function. Ind. Crops Prod. *219*, 119055.
8. Hu, O., Lu, M., Cai, M., Liu, J., Qiu, X., Guo, C.F., Zhang, C.Y., and Qian, Y. (2024). Mussel-bioinspired lignin adhesive for wearable bioelectrodes. Adv. Mater. *36*, 2407129.
9. Huang, H., Xu, C., Zhu, X., Li, B., and Huang, C. (2023). Lignin-enhanced wet strength of cellulose-based materials: A sustainable approach. Green Chem. *25*, 4995–5009.
10. Chen, S., Wang, Q., Shao, J., Li, X., Bian, Y., Jiang, S., Cao, Z., and Li, J. (2025). Decoupling of bonding strength and water retention in aqueous wood adhesive inspired by plant cell. ACS Nano *19*, 15876–15885.
11. Zhou, Y., Zeng, G., Zhang, F., Li, K., Li, X., Luo, J., Li, J., and Li, J. (2023). Design of tough, strong and recyclable plant protein-based adhesive via dynamic covalent crosslinking chemistry. Chem. Eng. J. *460*, 141774.
12. Anjum, S., Parks, K., Clark, K., Parker, A., Heveran, C.M., and Gerlach, R. (2025). Strengthening biopolymer adhesives through ureolysis-induced calcium carbonate precipitation. Sci. Rep. *15*, 3453.
13. Oni, O.V., and Chirdon, W.M. (2024). Evaluation of sustainable composites of sugarcane bagasse and combined algae-soy protein binders. Ind. Crops Prod. *213*, 118447.
14. Jin, J., Cheng, L., Chen, C., Li, Z., Hong, Y., Li, C., Ban, X., and Gu, Z. (2023). Synthesis, characterization, and application of starch-based adhesives modified with itaconic acid and N-hydroxyethyl acrylamide. Ind. Crops Prod. *196*, 116524.
15. Kan, Y., Kan, H., Bai, Y., Zhang, S., and Gao, Z. (2023). Effective and environmentally safe self-antimildew strategy to simultaneously improve the mildew and water resistances of soybean flour-based adhesives. J. Clean. Prod. *392*, 136319.
16. Chen, S., Liu, T., Guo, Y., Hao, X., Sun, L., Guo, C., Fan, Q., and Ou, R. (2024). Handling-friendly, waterproof, and mildew-resistant all-bio-based soybean protein adhesives with high-bonding performance via bio-inspired hydrophobic-enhanced crosslinking network. Ind. Crops Prod. *214*, 118583.
17. Huo, M., Yang, Z., Jin, C., Huo, S., Wu, G., Liu, G., and Kong, Z. (2024). Waterborne Lignin-Based epoxy resin: A green and effective chemical Cross-Linker to form soy Protein-Based wood adhesive with high performance. ACS Appl. Polym. Mater. *6*, 4078–4088.
18. Tian, Q. (2023). Preparation method and research progress of high performance adhesive for environmental friendly adhesive. China Pulp & Paper Industry *44*, 15–19.
19. Nordqvist, P., Khabbaz, F., and Malmström, E. (2010). Comparing bond strength and water resistance of alkali-modified soy protein isolate and wheat gluten adhesives. Int. J. Adhes. Adhes. *30*, 72–79.
20. Aladejana, J.T., Zeng, G., Zhang, F., Li, K., Li, X., Dong, Y., and Li, J. (2023). Tough, waterproof, and mildew-resistant fully biobased soybean protein adhesives enhanced by furfuryl alcohol with dynamic covalent linkages. Ind. Crops Prod. *198*, 116759.
21. Liu, H., Li, X., Pan, Z., Dai, L., Zhang, M., Shen, F., and Si, C. (2025). Lignin-based plugging hydrogel with high-temperature resistance and adjustable gelation. Adv. Compos. Hybrid Mater. *8*, 111.
22. Chang, J., Kan, Y., Han, S., Wei, S., and Gao, Z. (2024). Effects of dehydration time on performances of polyamidoamine-epichlorohydrin resin and its modified soybean-based adhesive. Int. J. Adhes. Adhes. *134*, 103813.
23. Hao, X., and Fan, D.B. (2018). Preparation and characterization of epoxy-crosslinked soy protein adhesive. J. Adhes. Sci. Technol. *32*, 2682–2692.
24. Du, Q., Hu, B., Shen, Q., Su, S., Wang, S., and Song, G. (2024). Creating tough Mussel-Inspired underwater adhesives from plant catechyl lignin. Chem. Eng. J. *482*, 148828.
25. Zhang, H.J., Zha, S., Wang, X., Xie, L., Liang, S., Zou, X., Liu, X., Dang, X., and Wang, X. (2023). Dual Cross-Linked Gelatin-Based adhesive for leather with low curing temperature and improved bonding strength. ACS Appl. Polym. Mater. *5*, 10515–10525.
26. Yu, H., Xia, Y., Jin, Z., Zhang, L., Liu, X., Chen, H., Wang, Z., Wang, S., and Shi, S. (2024). The analysis of response surface optimization and performance of cross-linked starch/tannic acid adhesive reinforced by phragmites fibers. Polym. Compos. *45*, 7495–7506.
27. Qie, R., Zajforoushan Moghaddam, S., and Thormann, E. (2024). Fully bio-based adhesive from chitosan and tannic acid with high water resistance. ACS Sustain. Chem. Eng. *12*, 4456–4463.
28. Ghahri, S., and Park, B.D. (2024). Amination and crosslinking of acetone-fractionated hardwood kraft lignin using different amines and aldehydes for sustainable bio-based wood adhesives. Bioresour. Technol. *399*, 130645.

29. Meng, T., Ding, Y., Liu, Y., Xu, L., Mao, Y., Gelfond, J., Li, S., Li, Z., Salipante, P.F., Kim, H., et al. (2023). In situ lignin adhesion for High-Performance bamboo composites. Nano Lett. *23*, 8411–8418.

30. Xu, X., Hu, W., Ke, Q., Liu, H., Li, J., and Zhao, Y. (2020). Bio-adhesives from unfolded soy protein reinforced by nano-chitosan for sustainable textile industry. Textil. Res. J. *90*, 1094–1101.

31. Zeng, G., Dong, Y., Luo, J., Zhou, Y., Li, C., Li, K., Li, X., and Li, J. (2024). Desirable strong and tough adhesive inspired by dragonfly wings and plant cell walls. ACS Nano *18*, 9451–9469.

32. Liu, T., Yang, Y., Yan, L., Lin, B., Dai, L., Huang, Z., and Si, C. (2024). Custom-designed polyphenol lignin for the enhancement of poly(vinyl alcohol)-based wood adhesive. Int. J. Biol. Macromol. *258*, 129132.

33. Li, X., Chen, S., Shao, J., Bai, M., Zhang, Z., Song, P., Jiang, S., and Li, J. (2024). From waste to strength: Tailor-made enzyme activation design transformation of denatured soy meal into high-performance all-biomass adhesive. Int. J. Biol. Macromol. *273*, 133054.

34. Zeng, H., Jin, T., Shi, S., Liu, L., Guo, H., Xie, L., Chai, X., Xu, K., Du, G., and Zhang, L. (2023). Boiling water resistant fully bio-based adhesive made from maleated chitosan and glucose with excellent performance. Int. J. Biol. Macromol. *253*, 127446.

35. Liu, J., Pan, B., Shen, J., and Yang, Y. (2022). Properties of dialdehyde starch modified soybean protein adhesive. Journal of University of Science & Engineering(Natural Science Edition) *35*, 51–58.

36. Gao, W., Fu, Z., Pan, W., Qin, C., Ning, C., Liu, M., Qin, Z., Li, Z., and Zhao, S. (2025). Dynamically crosslinking bio-inspired adhesives with high bond strength and multi-environmental adaptability for ultra-low temperature adhesion. Adv. Funct. Mater. *35*, e11884.

37. Li, R., Li, L., Qiu, W., Zhu, D.Y., Qiu, X., Ou, R., Liu, B., and Liu, W. (2025). Sustainable waterborne polyurethane adhesive with superstrong adhesion performance and excellent weatherability from biomass lignin and CO2 -based polyols. Adv. Funct. Mater. *35*, 2422605.

38. Zhao, C., Chu, Z., Mao, Y., Xu, Y., Fei, P., Zhang, H., Xu, X., Wu, Y., Zheng, M., and Liu, J. (2023). Structural characteristics and acid-induced emulsion gel properties of heated soy protein isolate–soy oligosaccharide glycation conjugates. Food Hydrocoll. *137*, 108408.

39. Liu, Y., Li, K., Tian, J., Gao, A., Tian, L., Su, H., Miao, S., Tao, F., Ren, H., Yang, Q., et al. (2023). Synthesis of robust underwater glues from common proteins via unfolding-aggregating strategy. Nat. Commun. *14*, 5145.

40. Zheng, G., Zhang, S., Wang, Y., Pan, A., Xu, B., Xu, Y., and Zhang, X. (2025). Preparation of a multifunctional bio-based adhesive inspired by the structure of dragonfly wings. Compos. B Eng. *298*, 112374.

41. Yang, S., Lian, Z., Zhu, T., Guo, X., Zhang, Q., Wang, H., and Jiang, L. (2025). Soybean protein isolate-oxidized fucoidan nanocomplexes: Structural and interaction characterization, quercetin delivery potential evaluation. Food Chem. *469*, 142528.

42. Chen, L., Liang, M., Qu, P., Sun, E., Yong, C., Jin, H., and Huang, H. (2025). Deep eutectic solvent-facilitated demethylation and depolymerization for producing highly reactive and antioxidative lignin. Int. J. Biol. Macromol. *321*, 146230.

43. Huo, H., Shen, J., Wan, J., Shi, H., Yang, H., Duan, X., Gao, Y., Chen, Y., Kuang, F., Li, H., et al. (2025). A tough and robust hydrogel constructed through carbon dots induced crystallization domains integrated orientation regulation. Nat. Commun. *16*, 6221.

44. Gao, X., Ma, R., Liu, Z., Wang, S., Wu, Y., and Song, G. (2024). Hydrodeoxygenation of lignin-derived phenols into cycloalkanes by atomically dispersed Pt-polyoxometalate catalysts. Appl. Catal. B Environ. Energy *352*, 124059.

45. Börcsök, Z., and Pásztory, Z. (2021). The role of lignin in wood working processes using elevated temperatures: An abbreviated literature survey. Eur. J. Wood Wood Prod. *79*, 511–526.

46. Zheng, J., Chen, L., Qiu, X., Liu, Y., and Qin, Y. (2023). Structure investigation of light-colored lignin extracted by Lewis acid-based deep eutectic solvent from softwood. Bioresour. Technol. *385*, 129458.

47. Wang, X., Xia, Q., Jing, S., Li, C., Chen, Q., Chen, B., Pang, Z., Jiang, B., Gan, W., Chen, G., et al. (2021). Strong, hydrostable, and degradable straws based on cellulose-lignin reinforced composites. Small *17*, 2008011.

48. Liang, Z., Xue, J., Yan, Q., Sun, Y., Luo, S., Zhu, Y., and Zhang, S. (2025). Advanced Dual-Cross-Linking strategy for upgrading Formaldehyde-Free olefin adhesives. Nano Lett. *25*, 2931–2938.

49. Wang, Y., Sun, X.S., and Wang, D. (2007). Effects of preheating treatment on thermal property and adhesion performance of soy protein isolates. J. Adhes. Sci. Technol. *21*, 1469–1481.

50. Nordqvist, P., Nordgren, N., Khabbaz, F., and Malmström, E. (2013). Plant proteins as wood adhesives: Bonding performance at the macro- and nanoscale. Ind. Crops Prod. *44*, 246–252.

51. Salas, C., Rojas, O.J., Lucia, L.A., Hubbe, M.A., and Genzer, J. (2013). On the surface interactions of proteins with lignin. ACS Appl. Mater. Interfaces *5*, 199–206.

52. Chen, X., Wang, X., Luo, X., Chen, L., Li, Y., Xu, J., Liu, Z., Dai, C., Miao, H., and Liu, H. (2024). Bamboo as a naturally-optimized fiber-reinforced composite: Interfacial mechanical properties and failure mechanisms. Compos. B Eng. *279*, 111458.

53. Han, S., He, Y., Ye, H., Ren, X., Chen, F., Liu, K., Shi, S.Q., and Wang, G. (2024). Mechanical behavior of bamboo, and its biomimetic composites and structural members: A systematic review. J. Bionic Eng. *21*, 56–73.